Publisher: GSA
Journal: GEOL: Geology
DOI:10.1130/G36454.1

Glacio-isostatic control on hypoxia in a high-latitude shelf basin

Tom Jilbert[1*], Daniel J. Conley[2], Bo G. Gustafsson[3], Carolina P. Funkey[2], and Caroline P. Slomp[1]

[1]*Department of Earth Sciences (Geochemistry), Faculty of Geosciences, Utrecht University, P.O. Box 80.021, 3508 TA Utrecht, The Netherlands*

[2]*Department of Geology, Lund University, Sölvegatan 12, S-223 62 Lund, Sweden*

[3]*Baltic Nest Institute, Baltic Sea Centre, Stockholm University, S-106 91 Stockholm, Sweden*

*Current address: Department of Environmental Sciences, P.O. Box 65, 00014 University of Helsinki, Helsinki, Finland; tom.jilbert@helsinki.fi

ABSTRACT

In high-latitude continental shelf environments, late-Pleistocene glacial overdeepening and early Holocene eustatic sea-level rise combined to create restricted marine basins with a high vulnerability to oxygen depletion. Here we show that ongoing glacio-isostatic rebound during the Holocene may have played an important role in determining the distribution of past hypoxia in these environments by controlling the physical exchange of water masses and the distribution of large-scale phosphorus (P) sinks. We focus on the Baltic Sea, where sediment records from a large, presently oxic sub-basin show evidence for intense hypoxia and cyanobacteria blooms during the Holocene Thermal Maximum (HTM). Using paleobathymetric modeling, we show that this period was characterized by enhanced deep-water exchange, allowing widespread phosphorus regeneration. Intra-basin sills then shoaled over a period of several thousand years, enhancing P burial in one of the sub-basins. Together with climate forcing, this may have caused the termination of hypoxia throughout the Baltic Sea. Similar rearrangements of physical and

Publisher: GSA
Journal: GEOL: Geology
DOI:10.1130/G36454.1

chemical processes likely occurred in response to glacio-isostatic rebound in other high-latitude shelf basins during the Holocene.

INTRODUCTION

Restricted basins of the coastal oceans are vulnerable to oxygen depletion, being frequently characterized by estuarine circulation and stagnation of deep water masses (Farmer and Freeland, 1983). Understanding the conditions under which such basins become hypoxic is crucial to understanding the role of natural versus anthropogenic processes in the present-day expansion of coastal hypoxia (Diaz and Rosenberg, 2008) and the drivers of widespread burial of organic carbon in the geologic past (Jarvis et al., 2011).

The eustatic transgression of the early Holocene created numerous restricted basins in the modern ocean, ranging in scale from the Black Sea to fjord and lagoon systems across the full latitudinal gradient. In particular, glacial erosion of high-latitude continental shelves during the late Pleistocene led to the development of restricted basins during subsequent sea level rise (Fig. 1a). Overdeepening of bedrock topography by ice streams on the margins of major ice sheets caused fjord formation in mountainous regions (Kessler et al., 2008) and the incision of 100 m scale ‘deeps’ in tectonic depressions such as the Baltic basin (Amantov et al., 2011) and the St. Lawrence valley (Nota and Loring, 1964).

The modern Baltic Sea comprises a number of discrete sub-basins, centered on incised deeps between intervening sills (Fig. 1b). The sub-basins are characterized by distinct oxygen regimes (Fig. 1c), making the Baltic an ideal location to study the controls on hypoxia in shelf basins. Water-mass stratification in the Baltic Proper is maintained by saline water inflows from the North Sea, which stagnate in the deeps and become severely hypoxic and even euxinic (Fig. 1c). In contrast, the deep waters of the Bothnian Sea are oxic and relatively fresh, because the

sills of the Åland Sea are too shallow to allow exchange of deep waters from the Baltic Proper, and because nutrient loading is more moderate in northern regions, leading to lower productivity and oxygen demand (Lundberg et al., 2009).

Glacio-isostatic rebound after the retreat of the late Pleistocene ice sheets progressed independently of eustatic sea level rise, leading to the continuous evolution of coastlines in the high latitudes. During the deglaciation itself, freshwater and brackish phases occurred in the Baltic basin (16–8.5 ka, Andrén et al., 2011), the St. Lawrence valley hosted the inland Champlain Sea (13–9 ka, Cronin et al., 2008), and Hudson Bay experienced the Tyrrell Sea marine invasion (8–6.5 ka, Bilodeau et al., 1990). Ongoing rebound after sea level stabilization led to the closure of the Champlain Sea, the progressive isolation of the Baltic (Gustafsson and Westman, 2002) and the shoaling of fjord basins in both hemispheres (Skei, 1988; Gallagher et al., 1989). In this study we demonstrate the importance of glacio-isostasy to oxygen and nutrient regimes in high-latitude shelf basins, using the Baltic Sea as a case study.

METHODS SUMMARY

Sediment Coring, Sampling and Chemical Analysis

Sediment cores were collected from sites LL19 in the Baltic Proper (58.8807°N, 20.3108°E, 169m water depth) and SR5 in the Bothnian Sea (61.0833°N, 19.5797°E, 126m water depth) during cruises with R/V Aranda in May/June 2009 and R/V Skagerak in October 2008 (Fig. 1b). All cores were sliced at 0.5–2 cm resolution in a nitrogen- or argon-filled glovebox. Dried and homogenized subsamples were analyzed by combustion for C_{org} after decalcification, and by ICP-OES after total digestion (HF/ $HClO_4$/HNO_3) for selected elements. A parallel series of samples was taken at 1–5 cm resolution in a dark lab for pigment analysis. Cold HPLC-grade acetone: methanol: milliQ water (80:15:5%) was applied to dried,

homogenized subsamples, and the filtered extracts were analyzed by high performance liquid chromatography (HPLC) for echinenone and zeaxanthin. Complete methodological details are given in the Data Repository. All raw elemental and pigment concentration data are presented in Table DR2.

Core Chronologies

LL19 has been comprehensively dated as described elsewhere (Jilbert and Slomp, 2013) by ^{210}Pb dating of the upper sediments and matching of the C_{org} profile of deeper sediments to Loss on Ignition (LOI) in the Pb pollution-isochrone/PSV-dated master core 372740–3 from the Gotland Deep (Lougheed et al., 2012). This chronology was used to determine the duration of the hypoxic interval during the Holocene Thermal Maximum (HI_{HTM}) in the Baltic Proper, and the timing of its termination at ~4.0 ka (Fig. DR1). For dating of SR5, six bulk-sediment radiocarbon dates were obtained from a nearby core (MSM-16/1–082–03: 61.0768°N, 20.6233°E) including 5 within an interval apparently corresponding to the HI_{HTM} (as determined by elevated C_{org} values). Equivalent depths in MSM-16/1–082–03 and SR5 were identified by matching the C_{org} profiles of the two cores. The duration of the HI_{HTM} at SR5 was then estimated by calibrating the oldest and youngest radiocarbon dates of the HI_{HTM} to calendar ages using the Marine13 calibration curve in Oxcal v4.2 (Bronk Ramsey, 2009), assuming a constant reservoir age (Fig. DR1). Complete details of the dating approach are given in the Data Repository.

Bathymetric Modeling

The bathymetric modeling is based on the empirical shore-level displacement model described in Påsse and Andersson (2005). These authors assumed glacio-isostatic uplift of Fennoscandia over the period 20 ka–present to be represented by a composite curve of one slow and one fast component, for which general mathematical expressions could be formulated.

Publisher: GSA
Journal: GEOL: Geology
DOI:10.1130/G36454.1

Taking into account eustatic sea level rise, the parameters of the expressions were fitted to empirical data on shore-level curves from 79 sites distributed across Scandinavia. We interpolated these parameters across a 2D grid of present day elevation in the Baltic region (2 by 1 min in longitude and latitude, respectively, www.io-warnemuende.de/iowtopo). Past elevation at any position on the grid was calculated by subtracting uplift and eustatic sea level rise from the present day value.

RESULTS AND DISCUSSION

The Baltic Sea became connected to the global ocean at around 8.5 ka (Andrén et al., 2011), during the period known as the Holocene Thermal Maximum (HTM, e.g., Renssen et al., 2009). Previous studies have demonstrated the subsequent occurrence of a hypoxic interval (here termed HI_{HTM}) in the Baltic Proper, which lasted for several thousand years (Zillén et al., 2008). The HI_{HTM} has been linked to high salinity and a strongly stratified water column (Zillén et al., 2008), resulting from both the drier, warmer climate of the HTM and from a deep configuration of the Danish Straits, which promoted saline water inflows into the Baltic Sea (Gustafsson and Westman, 2002). Our paleobathymetric modeling shows that the sills of the Åland Sea were also substantially deeper from 8–4 ka than during the late Holocene (Fig. 2). This suggests that the intermediate-salinity deep waters of the Baltic Proper during the HI_{HTM} may have extended into the Bothnian Sea.

High resolution sediment chemical records confirm that intensely hypoxic conditions were present in both the Baltic Proper and the Bothnian Sea during the HI_{HTM} (Fig. 3a). In both sub-basins, the sediments of the HI_{HTM} are characterized by high organic carbon (C_{org}) and molybdenum (Mo) contents, high organic carbon to total phosphorus (C_{org}/P_{tot}) ratios, and enhanced concentrations of the cyanobacterial pigments echinenone and zeaxanthin (Ech./C_{org}

Publisher: GSA
Journal: GEOL: Geology
DOI:10.1130/G36454.1

and Zeax./C_{org}), suggesting a stratified water column in which deep water hypoxia promoted sedimentary P regeneration and cyanobacteria blooms. The close correlation between the enhanced pigment concentrations and organic carbon contents indicate that the increase in organic matter in the sediment during the HI_{HTM} is due to increased production and preservation of marine organic matter. Laminated sediments characteristic of this interval have been observed in multiple cores from the Baltic Proper, and at least one other core from the Bothnian Sea (Zillén et al., 2008), suggesting that our records are broadly representative for these sub-basins. No reliable PSV age model yet exists for the Bothnian Sea, and radiocarbon dating of Baltic Sea sediments in general is hampered by reservoir age uncertainties and contamination with reworked carbon (Lougheed et al., 2013). However, the radiocarbon-estimated duration of the HI_{HTM} in the Bothnian Sea (~3.8 k.y., Fig. DR1) is similar to that of the HI_{HTM} in the Baltic Proper (3.3 k.y.), suggesting that the hypoxic intervals in the two sub-basins may have been co-eval.

The maximum intensity of hypoxia early in the HI_{HTM} was greater in the Bothnian Sea than in the Baltic Proper. C_{org}/P_{tot}, ratios and the concentrations of cyanobacterial pigments in Bothnian Sea sediments show maxima up to a factor 2–3 higher than the corresponding values in the Baltic Proper (Fig. 3a). Molybdenum to C_{org} scatter plots for the two sub-basins also suggest relatively stagnant conditions in the Bothnian Sea (Fig. 3b). The sediments of the Baltic Proper show tightly-correlated Mo and C_{org} concentrations between ~3.5 and 7% C_{org}, due to the efficient scavenging of Mo by organic matter in the presence of hydrogen sulfide and negligible basin reservoir effects (Jilbert and Slomp, 2013). In contrast, Bothnian Sea sediments of > 4% C_{org} (as recorded early in the HI_{HTM}, Fig. 3a) show Mo concentrations lower than predicted by

Publisher: GSA
Journal: GEOL: Geology
DOI:10.1130/G36454.1

the corresponding C_{org} value (Fig. 3b), suggesting partial depletion of water column Mo due to a longer deep water replacement time (Algeo and Lyons, 2006).

The HI_{HTM} in the Baltic Proper terminated abruptly at ~4.0 ka (Jilbert and Slomp, 2013), as determined by highly resolved paleomagnetic secular variation (PSV) dating (Lougheed et al., 2012). In contrast, the HI_{HTM} in the Bothnian Sea was characterized by a long-term decline in intensity after an initial maximum (Fig. 3a). A combination of isostatic and climatic factors may have led to the termination of the HI_{HTM} in both sub-basins. Our paleobathymetric reconstructions show a gradual shoaling of the Åland Sea sills from 8 ka to 4 ka (Fig. 2), which likely caused a progressive diminishment of the deep water exchange and simultaneous decline in hypoxia in the Bothnian Sea. This transition was also characterized by increasing P and iron (Fe) concentrations in the sediments of SR5, which continued after the termination of the HI_{HTM} (Fig. DR2). Although variability in mass accumulation rate at SR5 cannot be determined accurately with the available data, the increasing P and Fe concentrations strongly suggest an increase in the rate of P and Fe burial during this interval. Today, the Bothnian Sea acts as a sink for P exported from the surface waters of the Baltic Proper (Savchuk, 2005), through widespread incorporation of P into Fe oxyhydroxides in surface sediments, and into reduced Fe phosphates below the zone of anaerobic oxidation of methane deeper in the sediments (Slomp et al., 2013). We propose that the gradual severing of deep water exchange through the Åland Sea led to the progressive activation of this Fe-P sink, by improving oxygenation of the Bothnian Sea and allowing Fe oxyhydroxides to accumulate in the sediments.

The abrupt termination of the HI_{HTM} in the Baltic Proper may have been caused by a critical threshold of P burial rate in the Bothnian Sea being passed at ~4.0 ka, or by a climatic trigger acting in unison with enhanced P burial. Summer air temperatures during the HTM in the

Publisher: GSA
Journal: GEOL: Geology
DOI:10.1130/G36454.1

Baltic region declined after ~6 ka (Renssen et al., 2009). This long-term shift to cooler conditions may have been accompanied by increased precipitation in the Baltic catchment, reducing stratification of the Baltic Sea (Gustafsson and Westman, 2002) and favoring the termination of hypoxia.

Hypoxic conditions reappeared in the Baltic Proper during the Medieval Climate Anomaly (HI_{MCA}), and in the late 20th century (Fig. 3a). The absence of such conditions in the Bothnian Sea shows that reduced deep-water exchange through the Åland Sea limited the spatial extent of hypoxia during these intervals. Furthermore, hypoxia in the Baltic Proper occurred despite the active export of P into Bothnian Sea sediments. The rate of P burial in the Bothnian Sea in recent decades has been estimated at ~10–20 kton/yr (Wulff et al., 2001; Savchuk, 2005). During the same interval, the rate of external P input to the Baltic Sea as a whole has varied from ~40–70 kton/yr, much of which has entered the Baltic Proper directly (Gustafsson et al., 2012). Along with internal P regeneration, these high loads have maintained modern hypoxia despite the substantial export of P to the Bothnian Sea. Assuming regeneration and burial rates of P in the Baltic Proper to be similar during all hypoxic intervals (Jilbert and Slomp, 2013), this suggests that the HI_{MCA} was also partly driven by external P inputs, which more than compensated for P burial in the Bothnian Sea.

Glacio-isostatic rebound likely influenced the distribution of hypoxia in many high-latitude shelf basins during the Holocene. Our evidence from the Baltic Sea suggests hypoxia is favored when connection to the open ocean is restricted, but still sufficient to allow the development of a stratified water column, and when P sinks are limited in extent. A large body of evidence supports the influence of glacio-isostasy on hypoxia in similar environments. The initial marine incursion into Hudson Bay at ~8 ka was characterized by high-salinity deep

waters, a stratified water column and low-oxygen conditions (Bilodeau et al., 1990), suggesting an analogous scenario to the HI_{HTM} in the Baltic. The subsequent freshening and mixing of Hudson Bay may be partly explained by bathymetric changes due to glacio-isostatic rebound. In contrast, severe euxinia has developed in Norwegian fjords as their seaward sills have shoaled throughout the Holocene (Skei, 1988). Shoaling of the glacially-incised Lower St. Lawrence Estuary (Duchesne et al., 2010) likely also preconditioned the modern vulnerability of this system to stratification and hypoxia (Lefort et al., 2012).

Theoretically, complete glacio-isostatic isolation of shelf basins should lead to their freshening and mixing, as occurred during the closure of the Champlain Sea (Cronin et al., 2008). However, in fjord environments with an annual sea-ice cycle, hypersaline deep waters may form as a result of salt 'freeze-out' during ice growth. Glacio-isostatic rebound of such coastlines in Antarctica has been shown to create permanently stratified, hypoxic lakes after isolation from the ocean (Gallagher et al., 1989). Hence, the timeline of the response of hypoxia to glacio-isostatic change may vary strongly between different shelf basin environments.

ACKNOWLEDGMENTS

We thank the captain, crew and scientific participants aboard R/V Aranda (2009) for their assistance with the fieldwork. Ton Zalm, Arnold van Dijk and Helen de Waard are acknowledged for analytical assistance in Utrecht. Erik Smedberg is thanked for graphical work related to Fig. 1. Bryan Lougheed is thanked for discussions relating to dating of Baltic Sea sediments. Nina Reuss is thanked for assistance with pigment analysis. This research was funded by a Netherlands Organisation for Scientific Research (NWO) Vidi grant and a European Research Council (ERC) Starting Grant (278364) awarded to C.P.S., a Wallenberg

Scholar grant to D.J.C., Baltic Sea 2020 and the EU-BONUS projects HYPER and Baltic Gas.

REFERENCES CITED

Algeo, T.J., and Lyons, T.W., 2006, Mo-total organic carbon covariation in modern anoxic marine environments: Implications for analysis of paleoredox and paleohydrographic conditions: Paleoceanography, v. 21, no. 1, doi:10.1029/2004PA001112.

Amantov, A., Fjeldskaar, W., and Cathles, L., 2011, Glacial Erosion/Sedimentation of the Baltic Region and the Effect on the Postglacial Uplift, *in* Harff, J., Bjorck, S., and Hoth, P., eds., Baltic Sea Basin: Berlin, Springer-Verlag, p. 53–71.

Andrén, T., Bjorck, S., Andren, E., Conley, D., Zillén, L., and Anjar, J., 2011, The Development of the Baltic Sea Basin During the Last 130 ka, *in* Harff, J., Bjorck, S., and Hoth, P., eds., Baltic Sea Basin: Berlin, Springer-Verlag, p. 75–97.

Bilodeau, G., Devernal, A., Hillairemarcel, C., and Josenhans, H., 1990, Postglacial paleoceanography of Hudson Bay- stratigraphic, microfaunal, and palynological evidence: Canadian Journal of Earth Sciences, v. 27, no. 7, p. 946–963, doi:10.1139/e90-098.

Bronk Ramsey, C.B., 2009, Bayesian Analysis of Radiocarbon Dates: Radiocarbon, v. 51, no. 1, p. 337–360.

Cronin, T.M., Manley, P.L., Brachfeld, S., Manley, T.O., Willard, D.A., Guilbault, J.P., Rayburn, J.A., Thunell, R., and Berke, M., 2008, Impacts of post-glacial lake drainage events and revised chronology of the Champlain Sea episode 13–9 ka: Palaeogeography, Palaeoclimatology, Palaeoecology, v. 262, no. 1–2, p. 46–60, doi:10.1016/j.palaeo.2008.02.001.

Diaz, R.J., and Rosenberg, R., 2008, Spreading dead zones and consequences for marine ecosystems: Science, v. 321, no. 5891, p. 926–929, doi:10.1126/science.1156401.

Duchesne, M.J., Pinet, N., Bedard, K., St-Onge, G., Lajeunesse, P., Campbell, D.C., and Bolduc, A., 2010, Role of the bedrock topography in the Quaternary filling of a giant estuarine basin: The Lower St. Lawrence Estuary, Eastern Canada: Basin Research, v. 22, no. 6, p. 933–951.

Ehlers, J., Gibbard, P.L., and Hughes, P.D., eds., 2011, Quaternary Glaciations - Extent and Chronology: A Closer Look: Amsterdam, Elsevier, Developments in Quaternary Science Series, v. 15, 1108 p.

Farmer, D.F.H., and Freeland, H.J., 1983, The physical oceanography of fjords: Progress in Oceanography, v. 12, no. 2, p. 147–219, doi:10.1016/0079-6611(83)90004-6.

Gallagher, J.B., Burton, H.R., and Calf, G.E., 1989, Meromixis in an Antarctic fjord – A precursor to meromictic lakes on an isostatically rising coastline: Hydrobiologia, v. 172, p. 235–254, doi:10.1007/BF00031625.

Gustafsson, B.G., and Westman, P., 2002, On the causes for salinity variations in the Baltic Sea during the last 8500 years: Paleoceanography, v. 17, no. 3, doi:10.1029/2000PA000572.

Gustafsson, B.G., Schenk, F., Blenckner, T., Eilola, K., Meier, H.E.M., Mueller-Karulis, B., Neumann, T., Ruoho-Airola, T., Savchuk, O.P., and Zorita, E., 2012, Reconstructing the development of Baltic Sea eutrophication 1850–2006: Ambio, v. 41, p. 534–548, doi:10.1007/s13280-012-0318-x.

Jarvis, I., Lignum, J.S., Groecke, D.R., Jenkyns, H.C., and Pearce, M.A., 2011, Black shale deposition, atmospheric CO2 drawdown, and cooling during the Cenomanian-Turonian Oceanic Anoxic Event: Paleoceanography, v. 26, doi:10.1029/2010PA002081.

Jilbert, T., and Slomp, C.P., 2013, Rapid high-amplitude variability in Baltic Sea hypoxia during the Holocene: Geology, v. 41, p. 1183–1186, doi:10.1130/G34804.1.

Kessler, M.A., Anderson, R.S., and Briner, J.P., 2008, Fjord insertion into continental margins driven by topographic steering of ice: Nature Geoscience, v. 1, no. 6, p. 365–369, doi:10.1038/ngeo201.

Lefort, S., Gratton, Y., Mucci, A., Dadou, I., and Gilbert, D., 2012, Hypoxia in the Lower St. Lawrence Estuary: How physics controls spatial patterns: Journal of Geophysical Research, Oceans, v. 117, doi:10.1029/2011JC007751.

Lougheed, B.C., Snowball, I., Moros, M., Kabel, K., Muscheler, R., Virtasalo, J.J., and Wacker, L., 2012, Using an independent geochronology based on palaeomagnetic secular variation (PSV) and atmospheric Pb deposition to date Baltic Sea sediments and infer C-14 reservoir age: Quaternary Science Reviews, v. 42, p. 43–58, doi:10.1016/j.quascirev.2012.03.013.

Lougheed, B.C., Filipsson, H.L., and Snowball, I., 2013, Large spatial variations in coastal C-14 reservoir age: A case study from the Baltic Sea: Climate of the Past, v. 9, p. 1015–1028, doi:10.5194/cp-9-1015-2013.

Lundberg, C., Jakobsson, B.M., and Bonsdorff, E., 2009, The spreading of eutrophication in the eastern coast of the Gulf of Bothnia, northern Baltic Sea – An analysis in time and space: Estuarine, Coastal and Shelf Science, v. 82, p. 152–160, doi:10.1016/j.ecss.2009.01.005.

Nota, D.J.G., and Loring, D.H., 1964, Recent depositional conditions in the St. Lawrence River and Gulf – A reconnaissance survey: Marine Geology, v. 2, no. 3, p. 198–235, doi:10.1016/0025-3227(64)90040-4.

Påsse, T., and Andersson, L., 2005, Shore-level displacement in Fennoscandia calculated from empirical data: GFF, v. 127, p. 253–268, doi:10.1080/11035890501274253.

Renssen, H., Seppä, H., Heiri, O., Roche, D.M., Goosse, H., and Fichefet, T., 2009, The spatial and temporal complexity of the Holocene thermal maximum: Nature Geoscience, v. 2, p. 411–414, doi: 10.1038/NGEO513.

Savchuk, O.P., 2005, Resolving the Baltic Sea into seven subbasins: N and P budgets for 1991–1999: Journal of Marine Systems, v. 56, no. 1–2, p. 1–15, doi:10.1016/j.jmarsys.2004.08.005.

Skei, J.M., 1988, Framvaren – Environmental setting: Marine Chemistry, v. 23, no. 3–4, p. 209–218, doi:10.1016/0304-4203(88)90093-X.

Slomp, C.P., Mort, H.P., Jilbert, T., Reed, D.C., Gustafsson, B.G., and Wolthers, M., 2013, Coupled dynamics of iron and phosphorus in sediments of an oligotrophic coastal basin and the impact of anaerobic oxidation of methane: PLoS ONE, v. 8, no. 4, p. e62386, doi:10.1371/journal.pone.0062386.

Wulff, F., Rahm, L., Hallin, A.-K., and Sanberg, S., 2001, A nutrient budget model of the Baltic Sea, *in* Wulff, F., Rahm, L., and Larsson, P., eds., A systems analysis of the Baltic Sea: Berlin, Springer-Verlag, p. 353–372.

Zillén, L., Conley, D.J., Andren, T., Andren, E., and Bjorck, S., 2008, Past occurrences of hypoxia in the Baltic Sea and the role of climate variability, environmental change and human impact: Earth-Science Reviews, v. 91, no. 1–4, p. 77–92, doi:10.1016/j.earscirev.2008.10.001.

FIGURE CAPTIONS

Figure 1. Geography and hydrography of the Baltic Sea. A: Major glacially-incised shelf basins in the high northern latitudes. White dashed line = approximate extent of Laurentide and Scandinavian ice sheets at the Last Glacial Maximum (Ehlers et al., 2011). Red solid lines =

major fjord coastlines. Green = major flooded shelf basins with localized deeps and restricted connection to the open ocean. B: Bathymetric map of the Baltic Sea, showing the sub-basins relevant to this study (latitude and longitude in degrees N and E). Red dashed line indicates transect shown in B. B: Salinity and oxygen concentrations along the transect. Left to Right = South to North. BP = Baltic Proper, BS = Bothnian Sea, ÅS = Åland Sea. Black dashed line highlights the sills of the Åland Sea. Oxygen and salinity data was obtained from the Baltic Environmental Database. Negative oxygen indicates hydrogen sulfide.

Figure 2. Isostatic control on the geometry of the Åland Sea sills during the Holocene. A: temporal evolution (vertical axis) of water depth (shading) on a transect across the northern sill of the Åland Sea (horizontal axis). B: Elevation maps of the Åland Sea region at 1000 yr B.P. and 6000 yr B.P. The position of the transect in A is shown in red. Both plots are generated by interpolation of regional shoreline displacement curves from Påsse and Andersson (2005).

Figure 3. Sediment records from the Bothnian Sea (SR5) and Baltic Proper (LL19). A: Composite geochemical records from multi-core and gravity core samples. Hypoxic intervals, determined by enrichments in C_{org} and other parameters, are highlighted by horizontal gray bars. HI_{HTM} = Hypoxic Interval during the Holocene Thermal Maximum; HI_{MCA} = Hypoxic Interval during the Medieval Climate Anomaly; $HI_{Mod.}$ = Modern hypoxic interval. The depth corresponding to 4.0 ka is indicated in each core. Zeax. = zeaxanthin; Ech. = echinenone. Pigment concentrations are reported as µmol pigment per gram C_{org}. B: Molybdenum (Mo) versus organic carbon (C_{org}) crossplots of the gravity core data. Multi-core data are excluded due to the distorting influence of fresh organic matter in recently deposited sediments. Trendline in LL19 represents the linear regression for $3.5 < C_{org}$ (%) < 7, and is typical for weakly restricted, weakly euxinic basins. Gray field left of LL19 trendline (C_{org} <~3.5%) indicates sediments

deposited in non-euxinic conditions with minimal Mo enrichment. Trendline in SR5 represents the equivalent gradient to LL19, displaced left to account for an apparent lower threshold C_{org} value (~1%) for molybdenum enrichment at this site. Gray fields right of each trendline indicate sediments deposited under a water column depleted with respect to dissolved Mo, hence experiencing basin reservoir effects (Algeo and Lyons, 2006).

[1]GSA Data Repository item 2015xxx, including complete methods, Figures DR1 and DR2 and Tables DR1 and DR2, is available online at www.geosociety.org/pubs/ft2015.htm, or on request from editing@geosociety.org or Documents Secretary, GSA, P.O. Box 9140, Boulder, CO 80301, USA.

Combined Figures 1-3

Click here to download Figure: Combined figures 07.02.2015.pdf

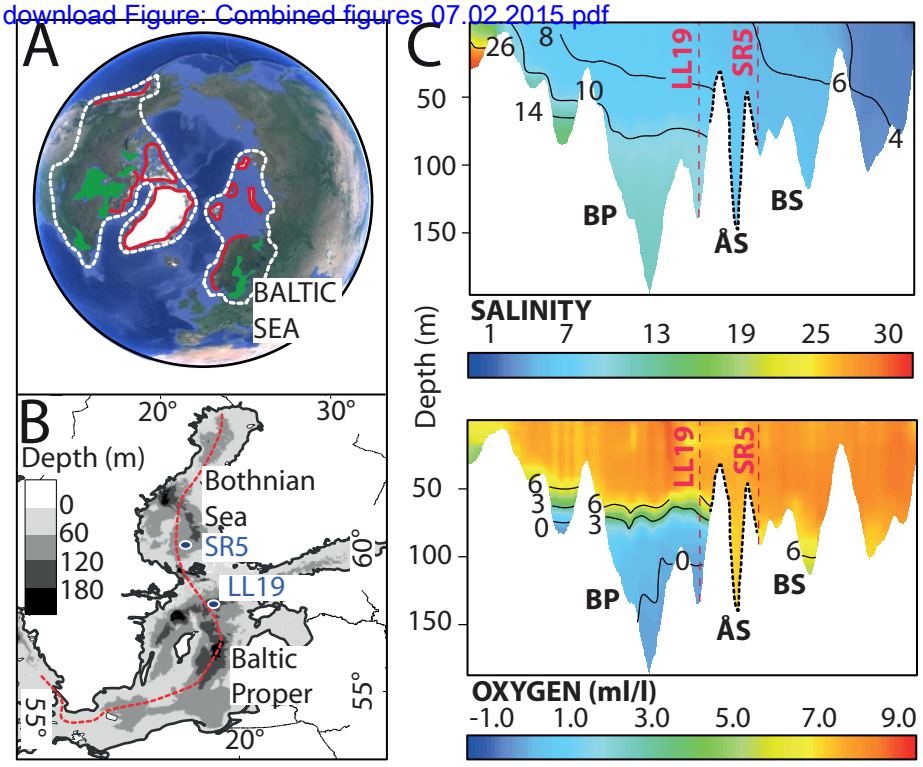

Figure 1

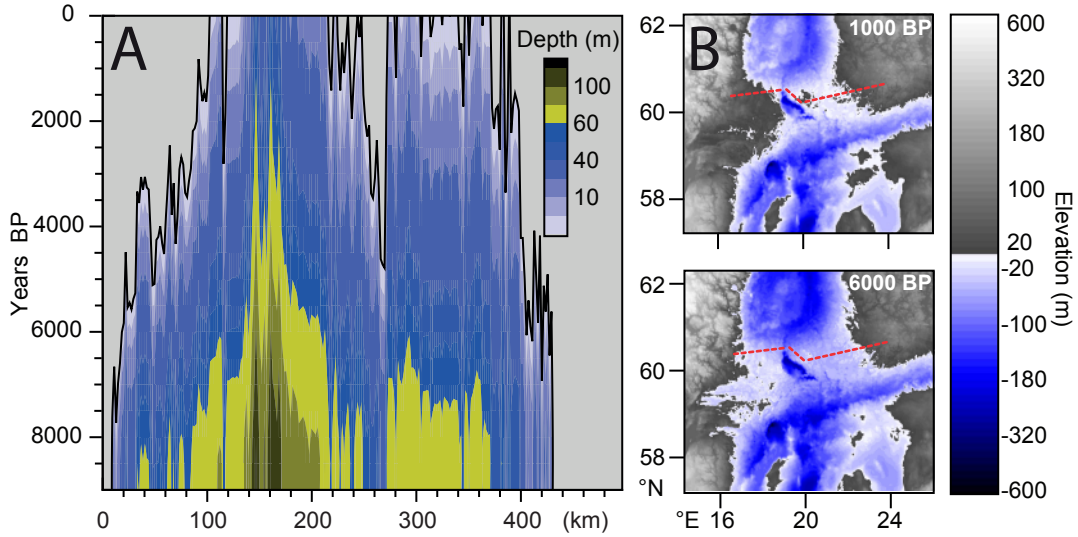

Figure 2

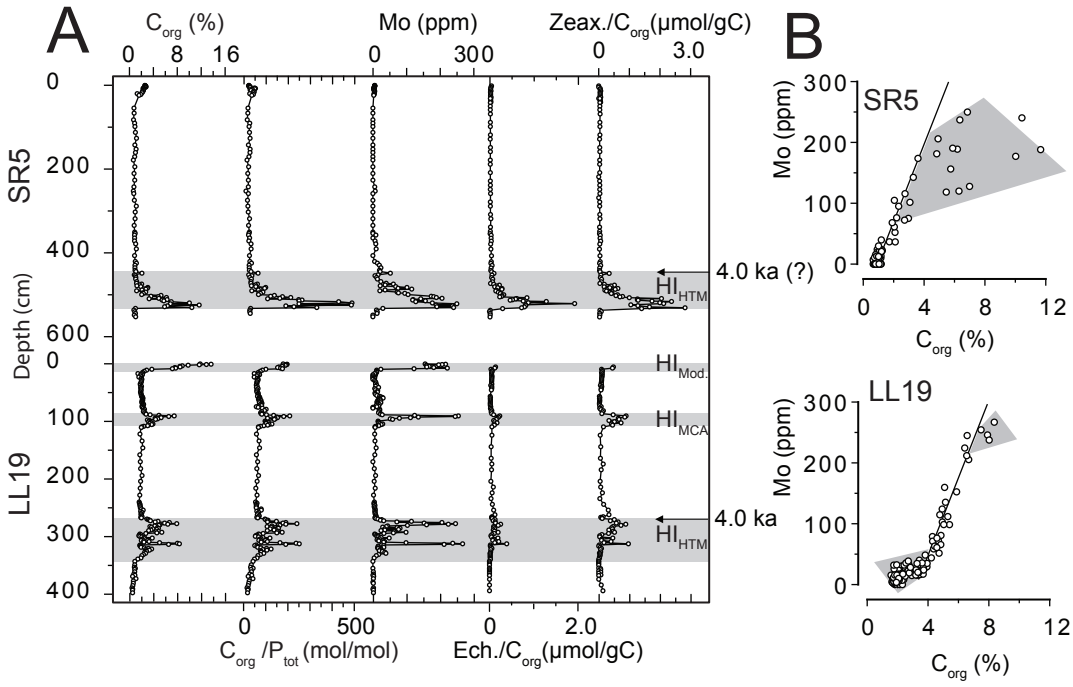

Figure 3

Data Repository Item for "Glacio-isostatic control on hypoxia in a high-latitude shelf basin"

Tom Jilbert*[1], Daniel J. Conley[2], Bo G. Gustafsson[3], Carolina P. Funkey[2], Caroline P. Slomp[1]

[1]*Department of Earth Sciences (Geochemistry), Faculty of Geosciences, Utrecht University P.O. Box 80.021, 3508 TA Utrecht, The Netherlands*

[2]*Department of Geology, Lund University, Sölvegatan 12, S-223 62 Lund, Sweden*

[3]*Baltic Nest Institute, Baltic Sea Centre, Stockholm University, S-106 91 Stockholm, Sweden*

**Corresponding author, now at: Department of Environmental Sciences, P.O. Box 65, 00014 University of Helsinki, Helsinki, Finland, tom.jilbert@helsinki.fi, Tel: +358919157923*

COMPLETE METHODS

Sediment coring, sampling and chemical analysis

Sediment multi-cores and gravity cores were collected from sites LL19 in the Baltic Proper (58.8807°N, 20.3108°E, 169m water depth) and SR5 in the Bothnian Sea (61.0833°N, 19.5797°E, 126m water depth) during cruises with R/V Aranda in May/June 2009 and R/V Skagerak in October 2008 (Fig. 1 of main article). All cores were sliced at 0.5-2 cm resolution in a nitrogen- or argon-filled glovebox. Sediment samples were freeze-dried and returned to the glovebox to be powdered and ground in an agate mortar. Subsamples were decalcified by shaking in excess 1M HCl, initially for 12 h and for a further 4 h after addition of new acid. The decalcified sediment was dried, ground in an agate mortar and analyzed by combustion for C_{org} by Fisons NA 1500 NCS (precision and accuracy <2% based on an atropine/acetanilide standard calibration and checked against internal laboratory standard sediments). A second subsample was dissolved in 2.5 ml HF (40 %) and 2.5 ml of an $HClO_4/HNO_3$ mixture, in a closed Teflon bomb at 90 °C for 12 h. The acids were then evaporated at 190 °C and the resulting gel was dissolved in 1M HNO_3, and analyzed for Mo (202.030 nm), P (177.495nm), and Al (308.215 nm) among other elements by ICP-OES (Ametek Spectro Arcos, precision and accuracy <5 %, based on calibration to standard solutions and checked against internal laboratory standard sediments). A parallel series of samples was taken at 1-5 cm resolution in a dark lab in preparation for pigment analysis. These samples were freeze-dried and ground, then mixed with cold HPLC-grade acetone: methanol: milliQ water (80:15:5%), sonicated and stored in a freezer (-20°C) overnight. Extracts were centrifuged and filtered at 0.45µm, and analyzed by high performance liquid chromatography (HPLC) on a Shimadzu Prominence HPLC equipped with an on-line photodiode array detector (SPD-M20A PDA) and an auto-sampler (Sil-10AF). See Funkey et

al. (2014) for more details. All raw elemental and pigment concentration data are presented in Table DR2.

Core chronologies

Multi-core and gravity core data were combined on the basis of overlaps in the geochemical profiles. LL19 has been comprehensively dated as described elsewhere (Jilbert and Slomp, 2013) by ^{210}Pb dating of the upper sediments and matching of the C_{org} profile of deeper sediments to Loss on Ignition (LOI) in the Pb pollution-isochrone/PSV-dated master core 372740-3 from the Gotland Deep (Lougheed et al., 2012a). This chronology was used to determine the duration of the hypoxic interval during the Holocene Thermal Maximum (HI_{HTM}) in the Baltic Proper, and the timing of its termination at ~4.0 ka (Fig. DR1). PSV dating is unavailable for SR5, and accurate radiocarbon dating of Baltic Sea sediments in general is hampered by reservoir age uncertainties and the potential for contamination with reworked carbon (Lougheed et al., 2012b). Therefore we focused on estimating the duration of the HI_{HTM} in the Bothnian Sea to assess the possibility of co-eval deposition with the HI_{HTM} in the Baltic Proper. Six bulk-sediment radiocarbon dates were obtained from core MSM-16/1-082-03 (61.0768°N, 20.6233°E) including 5 within the HI_{HTM} as determined by elevated C_{org} values. ^{14}C determinations were carried out at the Lund University Accelerator Mass Spectrometry (AMS) laboratory. MSM-16/1-082-03 is located very close to SR5 and shows a comparable C_{org} profile. Equivalent depths in MSM-16/1-082-03 and SR5 were thus identified by matching the C_{org} profiles of the two cores. The duration of the HI_{HTM} in SR5 was then estimated by calibrating the oldest and youngest radiocarbon dates of the HI_{HTM} to calendar ages using the Marine13 calibration curve in Oxcal v4.2 (Bronk Ramsey, 2009) (Fig. DR1). This calculation was performed assuming a reservoir age offset (ΔR) of 0 years and applying no correction for reworked carbon. Hence, the derived ages are expected to be older than the true ages of the sediments, potentially by >1000 years (Lougheed et al., 2012b). If

74 ΔR and the contribution of reworked carbon are assumed constant, the duration of the HI_{HTM}
75 in the Bothnian Sea is estimated at ~3.8 k.y., which is in the same range as the 3.3 k.y.
76 duration estimated for the HI_{HTM} in the Baltic Proper (Fig. DR1).

77 **Bathymetric modelling**

78 The bathymetric modelling is based on the empirical shore-level displacement model
79 described in Påsse and Andersson (2005). These authors assumed isostatic uplift of
80 Fennoscandia over the period 20 ka–present to be represented by a composite curve of one
81 slow and one fast component, for which general mathematical expressions could be
82 formulated. Taking into account eustatic sea level rise, the parameters of the expressions were
83 fitted to empirical data on shore-level curves from 79 sites distributed across Scandinavia. We
84 interpolated these parameters across a 2D grid of present day elevation in the Baltic region (2
85 by 1 minute in longitude and latitude, respectively, www.io-warnemuende.de/iowtopo). Past
86 elevation at any position on the grid was calculated by subtracting uplift and eustatic sea level
87 rise from the present day value. This simple means of calculation neglects possible
88 bathymetric changes due to sediment accumulation and erosion. However, this is only
89 relevant for deep basins areas, where accumulation is substantial, and not to the inter-basin
90 sill areas, which are dominated by bedrock.
91
92
93
94
95
96
97
98

99

100 **SUPPLEMENTARY FIGURES**

101

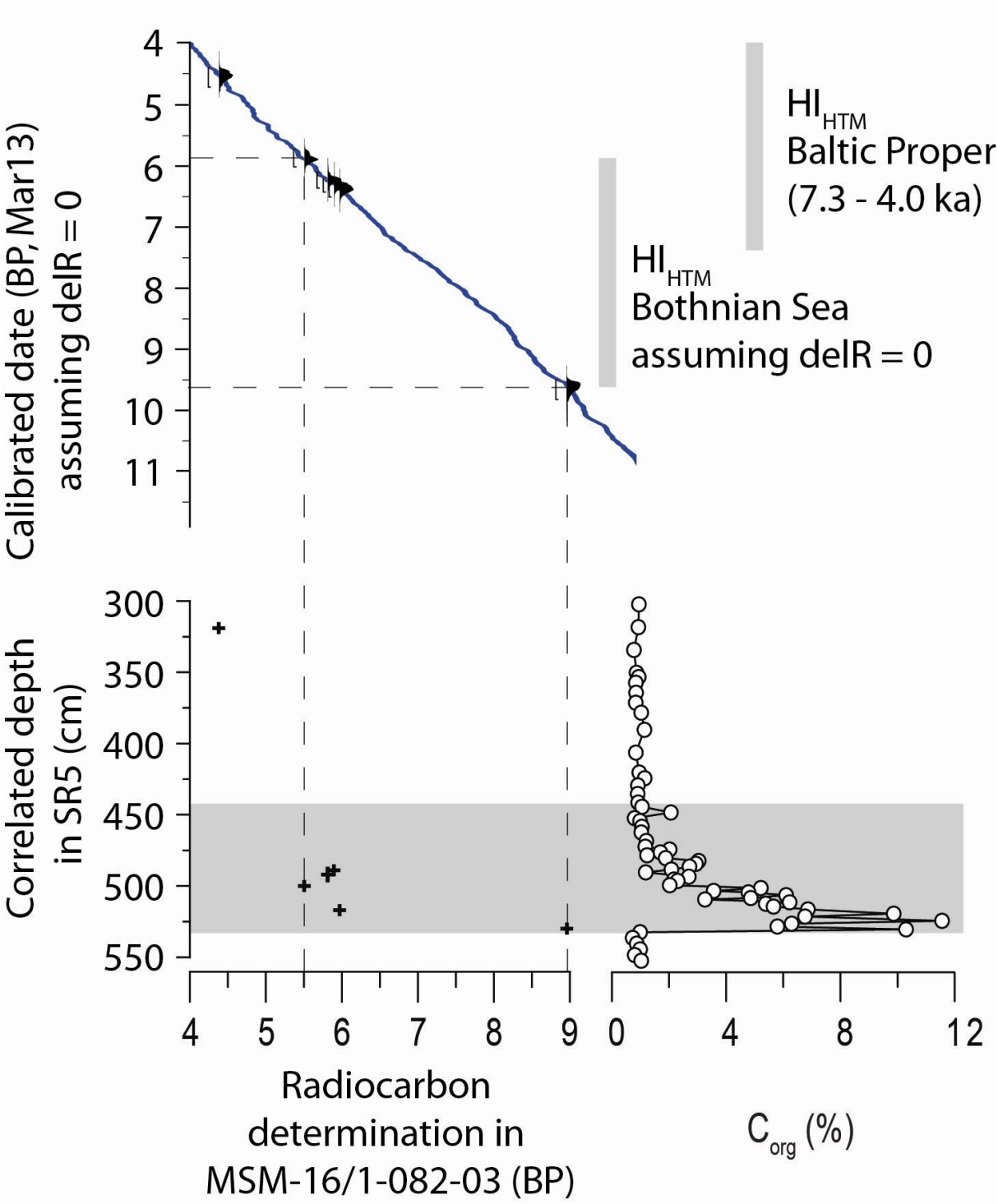

102

103

Figure DR1. Radiocarbon dating of Bothnian Sea sediments. Six bulk radiocarbon ages were determined in samples from core MSM-16/1-082-03. The equivalent depths of the six points in SR5 were determined by correlation of the C_{org} profiles of the two cores. Five of the points fall within the boundaries of the C_{org} excursion corresponding to the HI_{HTM} (indicated by the horizontal gray bar, 440-530 cm). Vertical dashed lines indicate the maximum radiocarbon age range of points within the HI_{HTM}. Calibration of this range to Marine13 (upper plot, assuming reservoir age offset (ΔR) = 0 and applying no correction for reworked carbon) yields a duration of the HI_{HTM} of ~3.8 k.y. The age and duration of the HI_{HTM} in the Baltic Proper (3.3 k.y. from 7.3 – 4.0 ka; Jilbert and Slomp, 2013) is shown for comparison. The HI_{HTM} in the Baltic Proper is dated by Paleomagnetic Secular Variation (PSV) and has an absolute age uncertainty of <0.5 k.y.

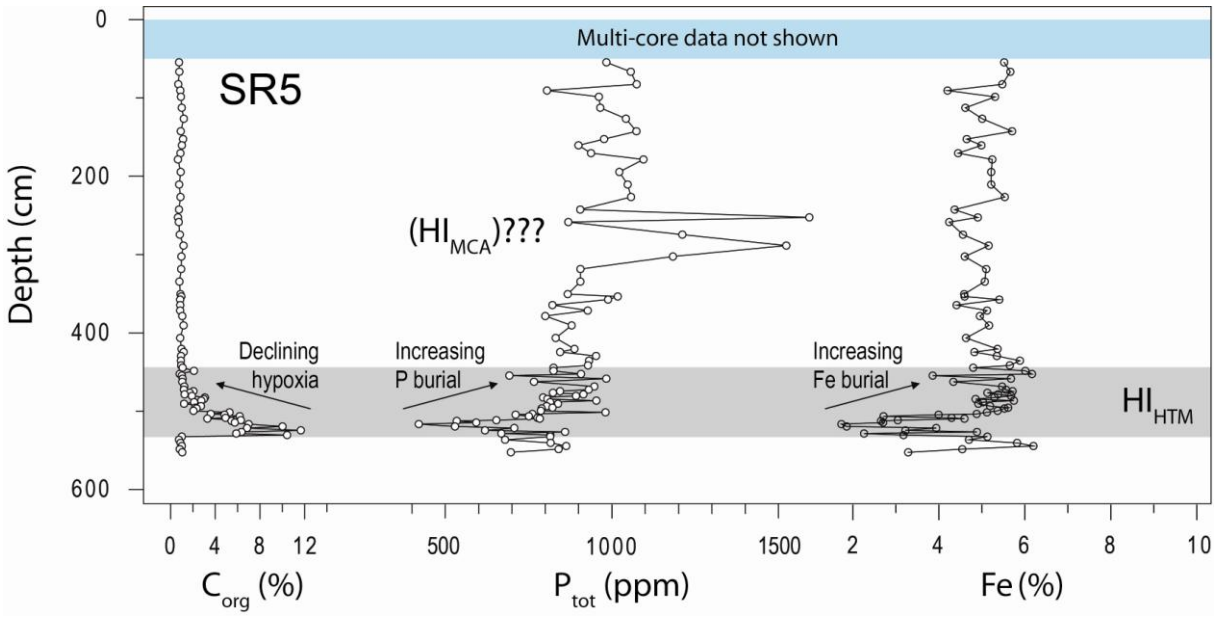

Figure DR2. C_{org}, P and Fe concentrations at SR5. The hypoxic interval during the Holocene Thermal Maximum (HI_{HTM}) is indicated by the horizontal gray bar. Multi-core data are not shown, in order to expand the scale on the P axis to highlight changes in the gravity core profile (extreme P concentrations in the surface sediments are related to modern-day cycling of P and are not representative for P concentrations upon burial).

SUPPLEMENTARY DISCUSSION

Changes in P burial rate in the Bothnian Sea

Assuming the termination of the HI_{HTM} (as determined by enhanced C_{org} values) at SR5 to occur at 4.0 ka, and the total duration of the HI_{HTM} at SR5 to be 3.8 k.y. (Fig. DR1), we calculated mean P burial rates for the HI_{HTM} and post-HI_{HTM} (i.e. 4.0 – present) intervals (Table DR1). These indicate a seven-fold higher mean P burial rate in the post-HI_{HTM} interval, the majority of the increase being caused by higher mass accumulation rates. However, mean P concentrations are also higher during the post-HI_{HTM} interval (Table DR1; Fig, DR2), suggesting a higher efficiency of P retention in Bothnian Sea sediments after the HI_{HTM}.

In the absence of high-resolution mass accumulation rate estimates it is difficult to accurately reconstruct P burial rates on shorter timescales. However, the depth profile of P concentration suggests that major changes in P burial may have occurred at SR5, both during and after the HI_{HTM}. The early part of the HI_{HTM} at SR5 is characterized by the lowest P content of the entire record (Fig. DR2), leading to an extremely high C_{org}/P_{tot} ratio (Fig. 3 of main article), indicative of efficient regeneration of P from the sediments under strongly reducing conditions. Hereafter, P concentrations first rise steeply, and then more steadily across the termination of the HI_{HTM} (Fig. DR2). The increase mirrors the decline in C_{org} concentration, and suggests that the P burial rate increased as hypoxia became less intense due to shoaling of the deep water exchange. Furthermore, a parallel increase in the Fe concentration (Fig. DR2) suggests that this excess P was buried primarily in association with Fe, either as Fe oxyhydroxide-bound P or vivianite, as observed in the Bothnian Sea today (Slomp et al., 2013).

Interestingly, strongly elevated P concentrations are observed at 250–350 cm depth in SR5 (Fig. DR2). We speculate that this interval may be co-eval with the HI_{MCA} in the Baltic Proper, and that the high P concentrations result from enhanced export of surface-water P across the straits of the Åland Sea, analagous to the situation during the modern hypoxic event (Savchuk, 2005). However, there is no way to confirm this theory until improved dating is available for the post-HI_{HTM} interval at SR5.

SUPPLEMENTARY DATA TABLES

Table DR1. Calculation of P burial rates at SR5. The depth and duration of the HI_{HTM} are estimated as described in Fig. DR1.

Period	Depth interval (cm)	Estimated duration (yr)	Mean sedimentation rate (cm/yr)	Mean dry bulk density (g/cm^3)	Mean mass accumulation rate ($g/cm^2/yr$)	Mean P_{tot} content (ppm)	Mean P_{tot} accumulation rate ($g/cm^2/yr$)
Post- HI_{HTM}	0-440	4000	0.110	0.399	0.044	1062	$4.56x10^{-5}$
HI_{HTM}	440-530	3800	0.024	0.379	0.009	808	$7.36x10^{-6}$

Table DR2. Raw sediment geochemical data used in Figure 3 of the main article. Note that some data in the figures are presented as ratios of the raw data in this table. Al data are also presented to allow readers to calculate Mo/Al (as used in other studies, e.g., Jilbert and Slomp, 2013). Depth scales represent combined multi-core and gravity core profiles. Blank cells = no data.

SR5

Bulk sediment elemental data					**Pigment data in µmol/g bulk sediment (note independent depth scale and C_{org} series from bulk elements)**			
Depth	C_{org}	P	Mo	Al	Depth	C_{org}	Ech.	Zeax.
cm	*%*	*ppm*	*ppm*	*%*	*cm*	*%*	*µmol/g*	*µmol/g*
0.25	2.6	2783	5	7.5	1.5	3.1	0.0014	0.0000
0.75	2.6	2802	6	7.5	4.5	3.1	0.0010	0.0000
1.25	2.7	2927	5	7.8	7.8	3.0	0.0008	0.0015
1.75	2.7	2875	6	7.4	10.5	2.7	0.0006	0.0013
2.50	2.7	2864	6	7.1	13.5	2.7	0.0009	0.0018
3.50	2.8	2397	4	5.8	16.5	2.6	0.0006	0.0011
4.50	2.7	2585	4	6.0	19.5	2.5	0.0006	0.0013
5.50	2.5	2212	4	7.8	22.5	2.4	0.0006	0.0012
6.50	2.4	1242	3	8.3	25.5	2.3	0.0005	0.0010
7.50	2.3	1096	3	7.9	28.5	2.0	0.0007	0.0013
8.50	2.4	1206	3	8.3	31.5	1.9	0.0005	0.0000
9.50	2.4	1564	3	7.7	34.5	1.8	0.0005	0.0009
10.50	2.3	2025	3	8.0	37.5	1.9	0.0005	0.0010
12.00	2.3	1777	3	8.1	40.5	1.8	0.0006	0.0011
14.00	2.3	1285	5	8.0	31.5	1.9	0.0004	0.0007
16.00	2.2	1166	5	8.1	41.5	2.1	0.0004	0.0008
18.00	2.1	1228	4	8.4	50.0	2.0	0.0004	0.0007
20.00	1.3	1208	4	8.7	58.5	2.1	0.0004	0.0007
22.00	1.9	1123	3	8.4	68.5	1.9	0.0004	0.0009
24.00	1.6	1120	3	8.6	88.5	1.9	0.0004	0.0007
54.5	0.8	983	<2	7.9	98.5	2.3	0.0004	0.0009
66.5	0.8	1057	<2	8.1	118.5	2.6	0.0005	0.0010

82.5	0.7	1074	<2	8.0	128.5	2.6	0.0004	0.0007
90.5	0.9	805	<2	5.9	148.5	2.5	0.0006	0.0008
98.5	0.9	961	<2	7.0	158.5	2.5	0.0005	0.0009
112.5	1.0	965	<2	6.7	178.5	2.5	0.0005	0.0008
126.5	1.2	1042	<2	7.0	188.5	2.5	0.0004	0.0007
142.5	0.9	1073	<2	8.1	208.5	2.3	0.0004	0.0008
152.5	1.1	976	<2	7.0	218.5	2.3		
160.5	1.0	900	<2	6.6	228.5	2.2	0.0004	0.0007
170.5	0.9	937	<2	6.6	238.5	2.3	0.0005	0.0008
178.5	0.7	1095	<2	7.8	248.5	2.6	0.0005	0.0008
194.5	0.9	1022	<2	7.4	258.5	2.3	0.0006	0.0009
210.5	0.8	1047	<2	7.7	268.5	2.2		
226.5	0.9	1057	<2	7.8	278.5	2.3	0.0004	0.0007
242.5	0.7	905	5	6.9	288.5	2.3	0.0005	0.0007
252.5	0.7	1593	7	6.3	308.5	2.4	0.0005	0.0008

Depth	C_{org}	P	Mo	Al	Depth	C_{org}	Ech.	Zeax.
cm	*%*	*ppm*	*ppm*	*%*	*cm*	*%*	*µmol/g*	*µmol/g*
258.5	0.7	869	<2	6.3	318.5	2.3	0.0007	0.0009
274.5	0.8	1211	<2	6.7	338.5	2.7	0.0006	0.0008
288.5	1.1	1523	<2	7.3	348.5	3.0	0.0006	0.0009
302.5	1.0	1183	<2	6.6	354.0	2.8	0.0004	0.0007
318.5	0.9	905	<2	7.2	358.0	2.7	0.0010	0.0013
334.5	0.8	905	<2	7.6	365.0	2.7	0.0010	0.0012
350.5	0.9	867	<2	6.8	372.0	2.7	0.0011	0.0017
353.5	1.0	1017	<2	7.1	379.0	2.9	0.0008	0.0010
357.5	0.9	988	9	8.3	391.0	2.9	0.0009	0.0007
364.5	0.9	821	<2	6.7	407.0	2.6	0.0012	0.0010
371.5	0.9	927	6	7.5	421.0	3.2	0.0013	0.0015
378.5	1.0	800	9	6.4	425.0	3.5	0.0011	0.0010
390.5	1.2	879	10	7.2	430.0	3.5	0.0020	0.0022
406.5	0.9	831	<2	6.7	436.0	3.2	0.0012	0.0010
420.5	1.0	888	5	7.2	442.0	2.8	0.0008	0.0008
424.5	1.2	844	13	6.6	445.0	3.0	0.0014	0.0013
429.5	0.9	952	19	.78	449.0	4.7	0.0047	0.0159
435.5	0.9	931	24	7.3	453.0	2.8	0.0016	0.0020

Depth	C_{org}	P	Mo	Al	Depth	C_{org}	Ech.	Zeax.
cm	*%*	*ppm*	*ppm*	*%*	*cm*	*%*	*µmol/g*	*µmol/g*
441.5	0.9	928	20	7.8	455.0		0.0486	0.1888
444.5	1.1	825	21	6.6	459.0	3.1	0.0015	0.0017
448.5	2.1	825	52	6.0	463.0	2.8	0.0020	0.0026
452.5	0.8	907	15	7.6	469.0	3.2	0.0021	0.0027
454.5	1.0	692	6	5.8	473.0	3.6	0.0008	0.0014

458.5	1.1	983	11	7.9	475.0	4.5	0.0043	0.0082
462.5	1.0	766	13	6.1	477.0	5.4	0.0122	0.0279
468.5	1.2	947	24	8.0	479.0	5.4	0.0087	0.0216
472.5	1.2	930	40	7.3	481.0	3.2	0.0037	0.0056
474.5	2.0	844	61	6.4	483.0	6.7	0.0124	0.0242
476.5	1.7	823	36	6.6	485.0	7.7	0.0219	0.0484
478.5	1.2	914	22	7.8	487.0	6.2	0.0175	0.0336
480.5	1.9	892	68	6.8	489.0	6.0	0.0092	0.0120
482.5	3.1	793	101	5.1	491.0	4.4	0.0063	0.0111
484.5	3.0	806	75	5.7	494.0	5.1	0.0101	0.0190
486.5	2.7	953	116	6.5	496.0	6.7	0.0168	0.0288
488.5	2.1	815	36	6.7	497.0	5.3	0.0130	0.0217
490.5	1.2	838	21	7.0	500.0	8.8	0.0285	0.0543
493.5	2.7	804	72	5.9	502.0	8.3	0.0236	0.0463
495.5	2.2	822	76	6.6	504.0	11.2	0.0303	0.0869
496.5	2.3	789	95	5.9	505.0	10.5	0.0243	0.0728

Depth *cm*	C_{org} *%*	P *ppm*	Mo *ppm*	Al *%*	Depth *cm*	C_{org} *%*	Ech. *µmol/g*	Zeax. *µmol/g*
499.5	2.0	787	105	6.1	507.0	13.2	0.1114	0.1314
501.5	5.3	981		5.2	509.0	15.3	0.0937	0.3126
503.5	3.6	761	174	5.0	510.0	11.8	0.0698	0.1498
504.5	4.8	711	181	4.0	512.0	12.4	0.0647	0.1569
506.5	6.2	751	189	3.0	513.0	11.1	0.0520	0.1434
508.5	4.9	776	206	4.2	515.0	11.7	0.0891	0.2032
509.5	3.3	783	142	5.0	516.0	12.8	0.1644	0.3043
511.5	6.3	653	120	3.5	519.0	16.0	0.1402	0.3188
512.5	5.5	534	118	2.7	521.0	18.3	0.3514	0.3870
514.5	5.7	593	156	2.6	524.0	14.7	0.1192	0.1535
516.5	7.0	420	128	1.7	526.0	15.5	0.1266	0.1976
519.5	10.0	529	177	1.9	529.0	17.8	0.1402	0.2942
521.5	6.8	707	250	3.1	531.0	17.1	0.1240	0.4814
524.5	11.7	619	188	2.9	533.0	9.4	0.0281	0.1323
526.5	6.4	859	237	4.3	537.0	2.0	0.0004	0.0008
528.5	5.9	668	190	2.3	540.0	2.5	0.0000	0.0021
530.5	10.4	815	240	3.4	544.0	2.5	0.0004	0.0008
532.5	1.0	815	30	6.3	548.0	2.3	0.0004	0.0009
536.5	0.7	679	11	6.1	553.0	3.0	0.0003	0.0008

Depth *cm*	C_{org} *%*	P *ppm*	Mo *ppm*	Al *%*	Depth *cm*	C_{org} *%*	Ech. *µmol/g*	Zeax. *µmol/g*
540.5	0.9	816	13	6.9				
544.5	1.0	863	12	7.2				

548.5	0.8	840	<2	6.7
552.5	1.0	697	<2	5.6

LL19

Bulk sediment elemental data					**Pigment data in µmol/g bulk sediment (note independent depth scale and C_{org} series from bulk elements)**			
Depth	C_{org}	P	Mo	Al	Depth	C_{org}	Ech.	Zeax.
cm	*%*	*ppm*	*ppm*	*%*	*cm*	*%*	*µmol/g*	*µmol/g*
0.25	11.83	1709	155	5.3	5.5	9.72	0.0133	0.0466
0.75	13.65	1794	216	5.1	7.5	8.38	0.0099	0.0375
1.25	12.87	1709	206	5.2	9.5	2.79	0.0009	0.0026
1.75	11.68	1570	196	5.6	11.5	2.46	0.0015	0.0030
2.50	9.82	1345	159	6.1	13.5	2.15	0.0013	0.0025
3.50	8.83	1284	160	6.4	15.5	2.10	0.0010	0.0019
4.50	8.44	1252	167	6.3	17.5	2.10	0.0010	0.0025
5.50	8.47	1370	160	6.1	19.5	2.01	0.0010	0.0020
6.50	7.59	1277	181	6.3	21.5	2.00	0.0011	0.0022
7.50	7.73	1194	221	6.4	23.5	1.97	0.0010	0.0019
8.50	7.18	1056	122	5.9	25.5	2.02	0.0011	0.0019
9.50	3.74	961	24	7.6	27.5	2.08	0.0010	0.0020
11.00	2.87	872	11	8.7	29.5	2.16	0.0011	0.0020
13.00	2.48	849	11	8.8	31.5	2.23	0.0011	0.0020
15.00	2.21	860	11	9.1	33.5	2.27	0.0011	0.0019
17.00	1.42	795	8	8.6	35.5	2.25	0.0012	0.0020
19.00	1.88	775	8	8.3	37.5	2.25	0.0006	0.0013
21.00	1.83	791	6	8.7	39.5	2.13	0.0011	0.0021
23.00	1.57	816	5	8.9	41.5	2.10	0.0010	0.0019
25.00	1.96	838	5	8.9	43.5	2.11	0.0010	0.0017
27.00	2.08	821	<2	8.4	45.5	2.15	0.0009	0.0016

Depth	C_{org}	P	Mo	Al	Depth	C_{org}	Ech.	Zeax.
cm	*%*	*ppm*	*ppm*	*%*	*cm*	*%*	*µmol/g*	*µmol/g*
29.00	2.01	804	5	8.4	68.5	2.5	0.0004	0.0005
31.00	1.99	856	7	8.8	70.5	2.6	0.0005	0.0005
33.00	1.92	821	9	8.5	72.5	2.5	0.0005	0.0008
35.00	1.80	786	8	8.1	74.5	2.7	0.0008	0.0022
37.00	1.84	825	11	8.5	76.5	3.0	0.0007	0.0013
39.00	2.01	846	8	8.7	77.5	3.0	0.0007	0.0011
41.00	1.88	837	17	8.8	79.5	3.2	0.0011	0.0022
43.00	1.93	764	5	8.3	81.5	2.9	0.0015	0.0044

45.00	1.93	819	8	8.7	83.5	3.0	0.0011	0.0037
47.00	1.94	841	14	8.9	86.5	3.0	0.0015	0.0031
49.00	1.85	793	13	8.5	88.5	4.3	0.0040	0.0200
51.00	1.92	750	6	8.2	90.5	8.4	0.0195	0.0754
53.00	1.95	777	8	8.3	92.5	7.5	0.0153	0.0639
55.00	2.00	777	12	8.0	94.5	6.8	0.0117	0.0434
56.50	2.03	834	20	8.6	96.5	5.8	0.0089	0.0385
57.50	2.17	789	24	7.9	98.5	3.5	0.0033	0.0118
58.50	2.15	762	28	7.9	100.5	3.3	0.0039	0.0169

Depth *cm*	C_{org} *%*	P *ppm*	Mo *ppm*	Al *%*	Depth *cm*	C_{org} *%*	Ech. *µmol/g*	Zeax. *µmol/g*
59.50	2.26	800	30	8-4	102.5	4.9	0.0082	0.0353
60.50	2.19	825	18	8.6	104.5	3.8	0.0040	0.0158
61.50	2.20	842	20	8.7	106.5	3.4	0.0037	0.0153
62.50	2.15	784	22	8.1	109.5	2.2	0.0012	0.0034
63.50	2.21	728	15	7.7	124.0	2.2	0.0012	0.0010
64.50	2.18	800	23	8.2	144.0	1.8	0.0007	0.0012
65.50	2.08	746	13	7.9	164.0	1.9	0.0007	0.0011
66.50	2.17	699	12	7.1	174.0	2.0	0.0010	0.0029
67.50	2.07	752	23	7.2	184.0	2.0	0.0009	0.0016
68.50	2.23	694	13	7.2	204.0	1.9	0.0006	0.0009
69.50	2.22	710	14	7.5	214.0	2.1	0.0018	0.0013
70.50	2.37	785	19	8.0	224.0	2.0	0.0012	0.0024
71.50	2.19	781	13	8.1	234.0	1.9	0.0007	0.0007
72.50	2.31	734	10	7.6	244.0	2.0	0.0013	0.0031
73.50	2.11	816	17	8.0	254.0	2.2	0.0021	0.0070
74.50	2.21	998	12	7.2	262.0	2.1	0.0026	0.0071
75.50	2.14	840	<2	6.7	265.5	2.3	0.0013	0.0034
77.00	2.31	706	<2	6.1	266.5	2.1	0.0010	0.0014
79.00	2.52	638	20	6.1	267.5	2.3	0.0012	0.0023

Depth *cm*	C_{org} *%*	P *ppm*	Mo *ppm*	Al *%*	Depth *cm*	C_{org} *%*	Ech. *µmol/g*	Zeax. *µmol/g*
81.00	2.37	648	20	6.4	268.5	2.5	0.0015	0.0029
83.00	2.33	737	18	6.7	270.5	4.0	0.0050	0.0203
85.00	2.52	848	17	8.7	272.5	4.5	0.0037	0.0169
86.50	2.71	879	23	8.7	274.5	5.0	0.0064	0.0314
87.50	2.79	875	23	8.6	276.5	8.0	0.0107	0.0458
88.50	3.46	865	28	8.2	278.5	7.9	0.0200	0.0700
89.50	4.93	938	124	8.0	280.5	5.3	0.0104	0.0383
90.50	7.49	928	254	6.5	282.5	3.5	0.0033	0.0166
91.50	6.57	936	245	6.6	284.5	5.8	0.0056	0.0245
92.50	5.15	886	135	7.2	286.5	5.3	0.0063	0.0237

93.50	5.30	894	112	7.3	288.5	3.8	0.0032	0.0126
94.50	4.29	1025	79	9.2	290.5	6.1	0.0068	0.0291
95.50	4.73	857	52	7.2	292.5	6.2	0.0120	0.0319
96.50	4.37	813	59	6.9	294.5	3.8	0.0041	0.0121
97.50	3.00				296.5	2.0	0.0011	0.0020
98.50	3.37				298.5	1.7	0.0005	0.0005
99.50	3.33	889	15	8.0	300.5	2.2	0.0010	0.0007
100.50	3.21	838	16	8.0	302.5	4.4	0.0083	0.0200
101.50	3.48	885	16	8.6	304.5	2.1	0.0018	0.0021

Depth *cm*	C_{org} *%*	P *ppm*	Mo *ppm*	Al *%*	Depth *cm*	C_{org} *%*	Ech. *µmol/g*	Zeax. *µmol/g*
102.50	3.68	838	17	7.7	306.5	2.2	0.0016	0.0020
103.50	3.41	867	20	7.6	308.5	3.3	0.0068	0.0131
104.50	3.93	793	29	7.1	310.5	3.0	0.0036	0.0052
105.50	3.71	836	25	7.9	312.5	10.3	0.0399	0.0994
106.50	3.16	753	17	7.3	314.5	2.6	0.0005	0.0005
107.50	3.03	860	17	8.4	316.5	1.9	0.0004	0.0000
108.50	2.40	810	8	8.5	318.5	2.4	0.0008	0.0012
109.50	2.08	799	6	8.8	320.5	3.0	0.0016	0.0026
110.50	1.98	765	7	8.4	322.5	3.3	0.0009	0.0019
122.00	1.76	780	5	8.6	326.5	3.3	0.0009	0.0021
134.00	2.11	781	6	8.4	328.5	3.2	0.0005	0.0008
146.00	2.23	800	10	8.5	329.5	3.4	0.0005	0.0015
158.00	1.74	773	6	8.8	331.5	2.8	0.0004	0.0013
170.00	1.82	739	<2	8.3	333.5	2.4	0.0004	0.0009
182.00	1.87	808	4	8.9	335.5	2.3	0.0003	0.0005
194.00	2.11	806	8	9.0	337.5	1.9	0.0004	0.0005
204.00	1.86	789	4	8.8	339.5	1.6	0.0003	0.0000

Depth *cm*	C_{org} *%*	P *ppm*	Mo *ppm*	Al *%*	Depth *cm*	C_{org} *%*	Ech. *µmol/g*	Zeax. *µmol/g*
216.00	1.80	842	7	9.2	342.5	1.0	0.0000	0.0000
228.00	1.73	735	2	8.4	343.5	1.2	0.0000	0.0000
240.00	1.63	777	4	8.9	345.5	1.2	0.0000	0.0000
242.00	1.67	713	3	8.2	347.5	1.1	0.0000	0.0000
244.00	1.78	807	4	9.2	349.5	0.9	0.0000	0.0000
246.00	1.75	777	6	8.9	354.5	1.1	0.0000	0.0000
248.00	1.83	823	4	9.2	355.5	1.1	0.0000	0.0005
250.00	1.82	822	5	9.2	357.5	1.0	0.0000	0.0005
252.00	1.97	640	6	7.3	359.5	1.0	0.0000	0.0000
254.00	2.30	743	7	8.1	361.5	1.0	0.0000	0.0005
256.00	1.87	809	6	9.1	363.5	1.0	0.0000	0.0000
258.00	2.10	796	7	8.5	366.5	0.8	0.0000	0.0004

260.00	1.94	779	6	8.9	367.5	0.9	0.0000	0.0000
262.00	1.94	811	8	8.6	374.0	0.9	0.0000	0.0000
264.00	2.01	733	9	8.0	384.0	0.8	0.0000	0.0004
265.50	2.11	812	10	8.7	394.0	0.5	0.0000	0.0004
266.50	1.89	818	7	8.9				
267.50	2.00	807	6	8.8				
268.50		820	9	8.8				

Depth	C_{org}	P	Mo	Al
cm	*%*	*ppm*	*ppm*	*%*
269.50	2.93	784	15	8.1
270.50	3.16	820	26	8.2
271.50	3.37	791	22	8.0
272.50	3.51	848	32	8.1
273.50	4.77	832	115	7.3
274.50	4.30	1028	71	7.9
275.50	6.67	904	205	7.0
276.50	5.88	853	152	7.1
277.50	7.91	849	246	6.4
278.50	6.41	868	224	7.0
279.50	5.09	839	160	7.7
280.50	4.94	779	103	7.2
281.50	4.22	854	44	8.1
282.50	3.43	833	40	8.1
283.50	3.69	768	29	7.9
284.50	4.68	774	72	7.1
285.50	4.85	795	81	7.4
286.50	3.94	847	35	8.4

Depth	C_{org}	P	Mo	Al
cm	*%*	*ppm*	*ppm*	*%*
287.50	4.59	829	76	7.7
288.50	3.61	678	35	7.1
289.50	3.21	776	24	8.1
290.50	4.84	793	66	7.4
291.50	4.44	749	63	7.2
292.50	5.41	802	99	7.3
293.50	4.58	789	61	7.9
294.50	2.74	800	33	8.6
295.50	1.75	664	5	8.0
296.50	1.90	683	7	7.9
297.50	1.67	727	11	7.7
298.50	1.57	740	15	8.3
299.50	1.73	843	12	9.1

300.50	2.06	781	15	9.0
301.50	2.52	744	24	8.4
302.50	3.82	828	48	8.4
303.50	2.48	810	19	8.3
304.50	2.10	742	14	8.5

Depth	C_{org}	P	Mo	Al
cm	*%*	*ppm*	*ppm*	*%*
305.50	2.15	753	12	8.4
306.50	1.98	746	17	8.5
307.50	2.39	772	18	8.5
308.50	3.28	788	35	8.1
309.50	2.43	788	32	8.5
310.50	5.03	790	99	7.4
311.50	8.02	874	237	6.8
312.50	8.36	858	267	6.6
313.50	6.54	887	212	7.0
314.50	1.77	809	26	7.6
315.50	1.75	897	32	8.3
316.50	1.81	779	16	8.5
317.50	1.95	764	16	8.6
318.50	1.94	784	32	7.6
319.50	2.50	829	14	8.8
320.50	3.19	796	16	8.3
321.50	3.71	772	24	8.0
322.50	2.69	797	23	8.6
323.50	3.33	818	20	7.9

Depth	C_{org}	P	Mo	Al
cm	*%*	*ppm*	*ppm*	*%*
324.50	2.76	936	19	8.2
325.50	2.84	925	28	7.9
327.00	2.55	824	35	8.3
329.00	2.70	766	39	7.6
331.00	2.35	795	17	7.7
333.00	2.07	824	10	8.9
337.00	1.92	816	4	9.0
339.00	1.40	736	<2	9.1
343.00	0.90	547	<2	7.7
345.00		652	<2	9.2
349.00	0.88	659	<2	9.2
353.00	0.82	672	<2	9.3
355.00	0.99	592	<2	8.5
357.00	0.88	674	<2	9.5

361.00	0.88	645	<2	9.1
365.00	0.73	667	2	9.6
367.00	0.91	639	<2	9.3
369.00	0.52	653	2	9.1

Depth *cm*	C_{org} *%*	P *ppm*	Mo *ppm*	Al *%*
373.00	1.09	667	<2	9.2
377.00	0.66	669	<2	9.3
379.00		645	<2	9.0
381.00	0.65	727	<2	9.9
385.00	0.57	710	<2	9.5
389.00	0.43	708	2	9.5
391.00	0.55	676	<2	9.2
393.00	0.52	700	2	9.6
397.50	0.53	763	2	10.1

SUPPLEMENTARY REFERENCES

Bronk Ramsey, C. B., 2009, Bayesian Analysis of Radiocarbon Dates: Radiocarbon, v. 51, no. 1, p. 337–360.

Funkey, C. P., Conley, D. J., Reuss, N. S., Humborg, C., Jilbert, T., and Slomp, C. P., 2014, Hypoxia sustains cyanobacteria blooms in the Baltic Sea: Environmental Science & Technology, v. 48, no. 5, p. 2598–2602.

Jilbert, T. and Slomp, C.P., 2013, Rapid high-amplitude variability in Baltic Sea hypoxia during the Holocene: Geology, v. 41, p. 1183–1186.

Lougheed, B.C., Snowball, I., Moros, M., Kabel, K., Muscheler, R., Virtasalo, J.J., and Wacker, L., 2012a, Using an independent geochronology based on palaeomagnetic secular variation (PSV) and atmospheric Pb deposition to date Baltic Sea sediments and infer C-14 reservoir age: Quaternary Science Reviews, v. 42, p. 43–58.

186 Lougheed, B.C., Filipsson, H.L. and Snowball, I., 2012b, Large spatial variations in coastal
187 C-14 reservoir age: A case study from the Baltic Sea. Climate of the Past, v. 9, p.
188 1015–1028.
189 Påsse, T. and Andersson, L., 2005, Shore-level displacement in Fennoscandia calculated from
190 empirical data. GFF, v. 127, p. 253–268.
191 Savchuk, O.P., 2005, Resolving the Baltic Sea into seven subbasins: N and P budgets for
192 1991–1999: Journal of Marine Systems, v. 56, no. 1–2, p. 1–15.
193 Slomp, C.P., Mort, H.P., Jilbert, T., Reed, D.C., Gustafsson, B.G., and Wolthers, M., 2013,
194 Coupled dynamics of iron and phosphorus in sediments of an oligotrophic coastal
195 basin and the impact of anaerobic oxidation of methane: PLoS ONE, v. 8, no. 4, p.
196 e62386.
197